metals

MDPI

Article

Effects of Rare Earth Elements on Microstructure and Mechanical Properties of H13 Die Steel

Rongchun Chen [1], Zhigang Wang [1,*], Jianguo He [2], Fusheng Zhu [3] and Chunhong Li [3]

[1] School of Material Science and Engineering, Jiangxi University of Science and Technology, Ganzhou 341000, China; crclss2017@163.com
[2] Special Steel Institute, Central Iron & Steel Research Institute, Beijing 100081, China; hejianguo@nercast.com
[3] Department of R&D and Manufacturing, Longnan Longyi Heavy Rare Earths Technology Co., Ltd., Ganzhou 341700, China; ph16162008@126.com (F.Z.); chli348@163.com (C.L.)
* Correspondence: zgwang2013@jxust.edu.cn; Tel.: 07-918-314-422

Received: 20 June 2020; Accepted: 7 July 2020; Published: 9 July 2020



Abstract: The effects of rare earth (RE) elements on the carbide distribution, transformation temperature, and mechanical properties of H13 die steels after annealing were systematically investigated by scanning electron microscopy, electron probe microanalysis, and transmission electron microscopy. The results indicated that the addition of RE elements is helpful in increasing the fraction of the disrupted $M_{23}C_6$ carbide along the grain boundaries, hindering the migration of grain boundaries and improving the crack-formation and expansion resistance of the carbides in the tensile process. With the addition of RE, the Ac_3 temperature increased by 11.4 °C and the diffusion of carbon atoms was pinned during the austenitizing process. Moreover, the carbides were modified by rare earth elements, and RE-inclusion promoted the transition of brittle-type failure to ductile-type failure. Therefore, the impact energy, hardness, and ultimate tensile strength improved significantly in the RE-modified H13 die steels.

Keywords: H13 die steel; carbides; mechanical properties; RE-inclusion

1. Introduction

H13 steel is a hot working die steel, which is widely used in hot pressing, hot extrusion, and casting of molds as it exhibits high hardenability, strong oxidation resistance, and excellent thermal fatigue performance [1–3]. With the increasingly complex application environment of H13 die steel, the mechanical properties of these steels are required to be improved for industrial applications [4,5]. The mechanical properties of such steels depend largely on the type, shape, size, and distribution of inclusions and carbides.

To further improve the mechanical properties of H13 steel, various studies have focused on the micro-alloying of H13 die steel. RE elements are referred to as 'industrial vitamins', and their effects on steel purification have been widely studied in the process of smelting [6–9]. With the improvement of refining technology, the requirements for clean steel have basically been met, and RE micro-alloying has become a key technique for developing high-quality die steels. The Gibbs free energy of RE elements is very low at high temperature. Therefore, these elements combine easily with oxygen and sulfur. Stable spherical RE-inclusions are formed with the addition of RE elements. Thus, the harmful effects of traditional inclusions are prevented, and the mechanical properties are significantly improved [10,11]. Trace RE elements generally occupy lattice points through vacancy diffusion in micro-alloyed steels [12]. Trace amounts of solid solution occurs in the steel, but yields considerable improvement in the mechanical properties, purifies the grain boundaries, shifts the continuous cooling transformation curve, and changes the critical transformation temperature

of the steels [13]. Recently, RE elements have been applied to many steels in order to change the carbide morphology and obtain a good carbide distribution in the matrix [14]. The segregation of the RE at grain boundaries purifies the boundaries, reduces the interfacial energy, and promotes carbide precipitation [6,15]. Wang reported that globular carbide had high toughness and crack propagation resistance [16]. Moreover, the addition of Ce promotes the segregation of W and Mo in tool and die steels, reduces the content of primary carbides, and refines the carbides [17]. Boccalini reported that RE is conducive to the formation of M_6C carbides [18,19]. However, full verification of the RE micro-alloying effects in H13 die steel is difficult due to the larger radii compared with iron atoms and the small amount of solid solution.

In this work, the effects of RE (yttrium, lanthanum, and cerium) on the microstructure and mechanical properties in H13 die steel were systematically analyzed by means of optical microscopy (OM), scanning electron microscopy (SEM), electron probe microanalysis (EPMA), and transmission electron microscope (TEM). This study evaluated the mechanism of RE micro-alloying modification and lays the foundation for broadening the application of rare earth micro-alloying in high-alloy-modified special steels.

2. Materials and Methods

H13 and RE-H13 die steels were designed [2,11,14] and fabricated with a 25-kg capacity medium-frequency induction furnace, the corresponding chemical compositions (see Table 1) was determined by inductively coupled plasma mass spectroscopy (ICPMS; PE ELAN9000, PerkinElmer, Waltham, MA, USA). The amount of solid solution RE was 0.0014%. The casting billet was heated for 1 h at 1150 °C, the final forging temperature was about 750 °C, and the ingots were all air-cooled to room temperature after forging. Subsequently, the forging blank was subjected to ultrafining treatment and annealing. The samples were heated to 850 °C during spheroidizing annealing for 4 h, then cooled to 750 °C for stress relief annealing for 4 h, and then cooled to room temperature in the furnace.

Table 1. The chemical composition of the test steels (wt.%).

Element (wt.%)	C	Si	Mn	Cr	Mo	V	P	S	O	N	RE
H13	0.38	0.99	0.37	5.1	1.36	1.07	0.011	0.003	0.0009	0.0046	-
RE-H13	0.39	1.04	0.38	5.1	1.34	1.04	0.012	0.003	0.0007	0.0045	0.0014

In preparation for microstructural characterization, the specimens were mechanically polished and etched with a 4% nital solution. The morphology of carbides was examined via field-emission scanning electron microscopy (FE–SEM; Carl Zeiss AG, Jena, Germany). After the samples were polished only, the distribution of the carbides was observed by means of a JXA8230 EPMA (Japan Electron Optics Ltd., Tokyo, Japan). Carbides were identified using a FEI Tecnai G2 F20 (Thermo Fisher Scientific, Waltham, MA, USA) TEM operated at 200 kV with a point-to-point resolution of 0.24 nm. TEM samples were first mechanically polished to thicknesses of approximately 50 μm, followed by ion–beam milling in a Gatan 691 precision ion polishing system (PIPS) (CBI, Scotia, NY, USA) at 5 kV with a final polishing step of 1 kV.

The tensile properties of the investigated steels after annealing were also evaluated at room temperature. Round bar tensile samples (gage length: 25 mm) were prepared in accordance with the GB/T 228.1–2010 standard. The samples were then tested (strain rate: 2 mm/min) on an electronic universal testing machine (UTM5105X, Suns Technology Co., Ltd, Shenzhen, China). The tensile properties were determined at room temperature and to ensure accuracy of the test data, each sample in the heat treatment state was tested twice. Moreover, impact toughness testing was performed on a liquid crystal cast iron pendulum impact test machine (PTM1500–BLZ, Suns Technology Co., Ltd., Shenzhen, China). Charpy V-notch impact samples were processed in accordance with NADCA (North American Die Casting Association) process specifications. The longitudinal toughness energy was measured. Each sample was tested three times, and the average impact energy was calculated

from the measured values. Furthermore, Vickers hardness measurements on the samples employed a load and holding time of 3 kgf and 15 s, respectively.

The transformation temperature of the H13 and RE-H13 die steels was investigated using a DIL805A type thermal expansion instrument (Baehr-Thermo, New Castle, Germany). Cylindrical ϕ 4 × 10 mm samples were cut from material in the annealed state. Both sections were perpendicular to the sides and all surfaces were polished. To prevent oxidative decarburization, the samples were heated and cooled under vacuum. The phase transition point Ac_3 was determined in accordance with YB/T 5127–1993 (2005). The test parameters were as follows: the temperature was increased at 10 °C/s to 600 °C, then at 0.05 °C/s to 1050 °C, and held at this temperature for 300 s. The material was then cooled at 0.1 °C/s to 600 °C and subsequently cooled at 10 °C/s to room temperature.

3. Results and Discussion

3.1. Effect of Rare Earth on Mechanical Properties

As shown in Figure 1a, the impact energy of the H13 die steel after annealing increased significantly with the addition of RE (longitudinal impact energy increases by 43.7% from 6.4 J to 9.2 J). Similarly, the hardness of the steel increased by 6.9% (from 205.1 HV to 219.3 HV), as shown in Figure 1b. Figure 1c,d shows the tensile properties of the tested steels after annealing. For a RE content of only 0.0014 wt.%, the ultimate tensile strength (UTS) of the RE-H13 die steel increased by ~50 MPa. These results show that the elongation rate decreased by 8% with increasing UTS, whereas the reduction in area was almost constant.

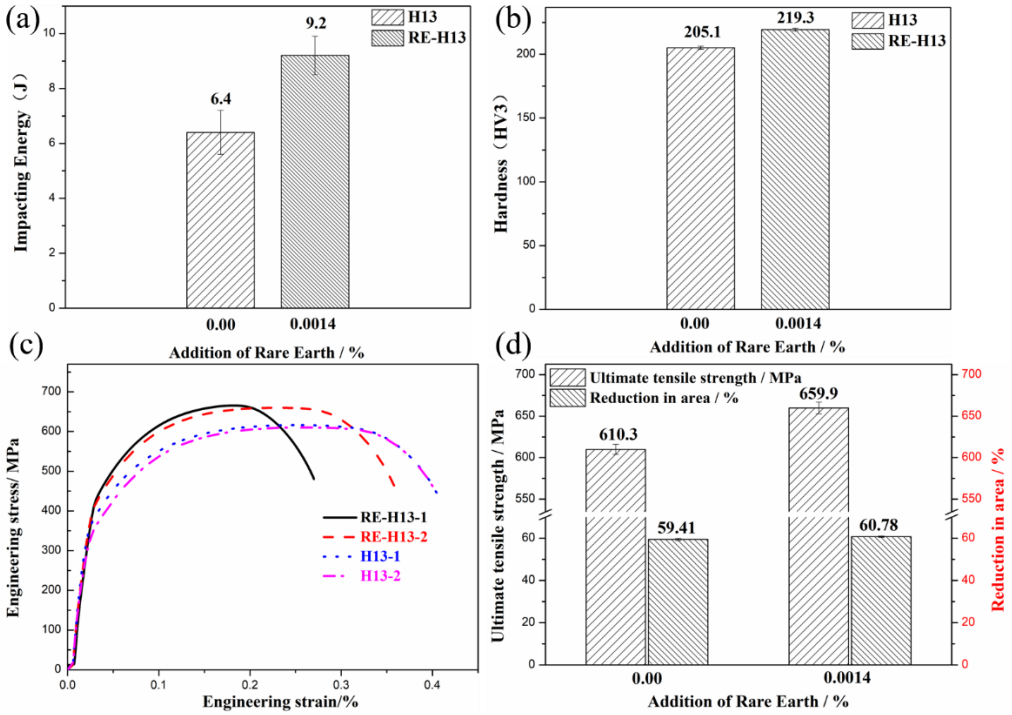


Figure 1. Mechanical properties of tested steels after annealing: (**a**) longitudinal impact energy, (**b**) hardness, (**c**) engineering stress–strain curves of annealed samples, and (**d**) tensile properties of annealed samples.

3.2. Effect of Rare Earth on Microstructure

The H13 die steel contains significant amounts of Cr, Mo, and V alloying elements, which form considerable carbides and nitrides with iron, carbon, and nitrogen. The microstructure of the tested steels was investigated by means of OM (Zeiss Axio Scope.A1; Carl Zeiss AG, Jena, Germany), SEM, and EPMA. The micrographs presented in Figure 2a,c show that numerous carbides occurred in the H13

die steel after annealing. A small number of carbides were distributed along the grain boundaries and most carbides were randomly distributed in the matrix. However, the fraction of carbides perfectly aligned along the grain boundaries increased considerably with the addition of RE (Figure 2b,d). To clarify the difference of large size carbides, the distribution of carbides was obtained by means of EPMA. As shown in Figure 2e, the result shows that most of the large white carbides were randomly distributed in the matrix. However, with the addition of RE, almost all large carbides were distributed along the grain boundaries in RE-H13 die steel. As shown in Figure 2g,h, this diagram explains the effects of RE on the distribution of large carbides along the grain boundaries. Hufenbach has reported a similar disruption of the carbide network along grain boundaries after a critical RE addition was reached [20]. However, there was no effect of RE on the distribution of nanoscale carbides.

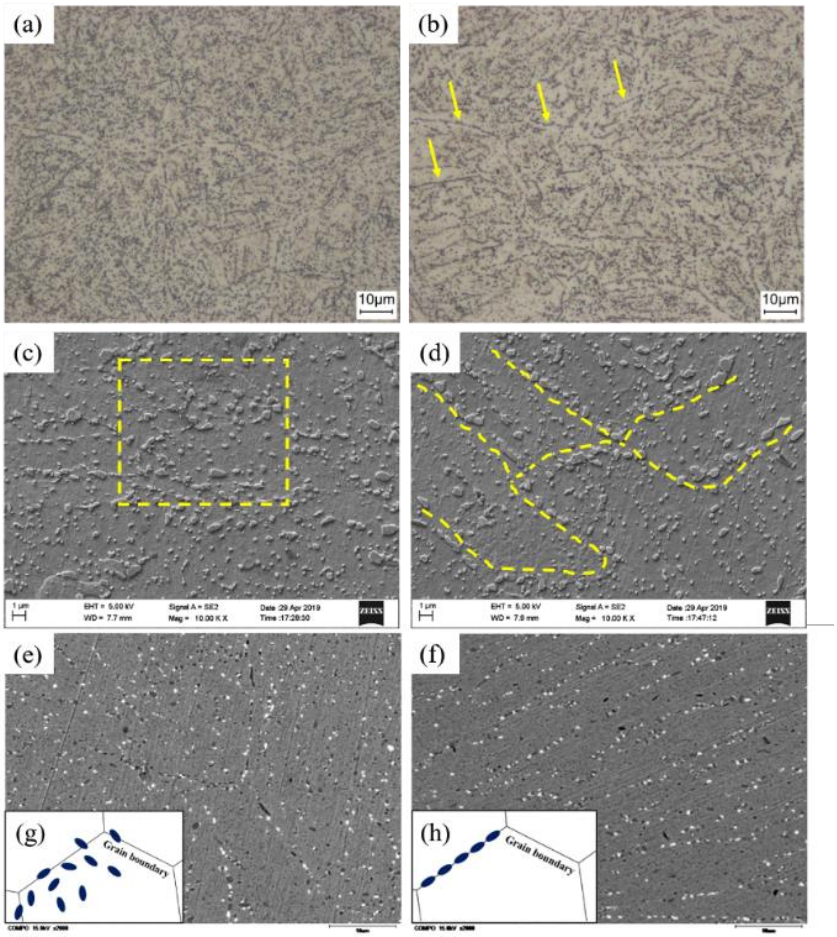


Figure 2. Distribution of carbides after annealing: (**a**), (**c**), and (**e**) H13 die steel; (**b**), (**d**), and (**f**) RE-H13 die steel; Diagram showing the carbide distribution and morphology of the (**g**) H13 die steel and (**h**) RE-H13 die steel.

Furthermore, to determine the type of carbides, TEM micrographs of carbides in RE-H13 die steel were investigated. As shown in Figure 3a, a considerable number of precipitates can be observed. Moreover, the effect of RE on large carbides was confirmed and almost all large carbides were distributed along the grain boundaries in the RE-H13 die steel. There were three types of carbides in the RE-H13 die steel after annealing: the type 1 carbide was distributed in intragranular; the type 2 carbide was distributed along the grain boundaries, and the type 3 carbide was nanoparticle. The corresponding selected area electron diffraction (SAED) pattern and energy disperse spectroscopy (EDS) analysis of the type 1 precipitate are shown in Figure 3c,d, which indicate that the complex

precipitate had an orthorhombic crystal structure, and was rich in Fe and Cr with a small amount of Mo and V. Therefore, the type 1 carbide was identified as Cr_7C_3 with the size of about 500 nm.

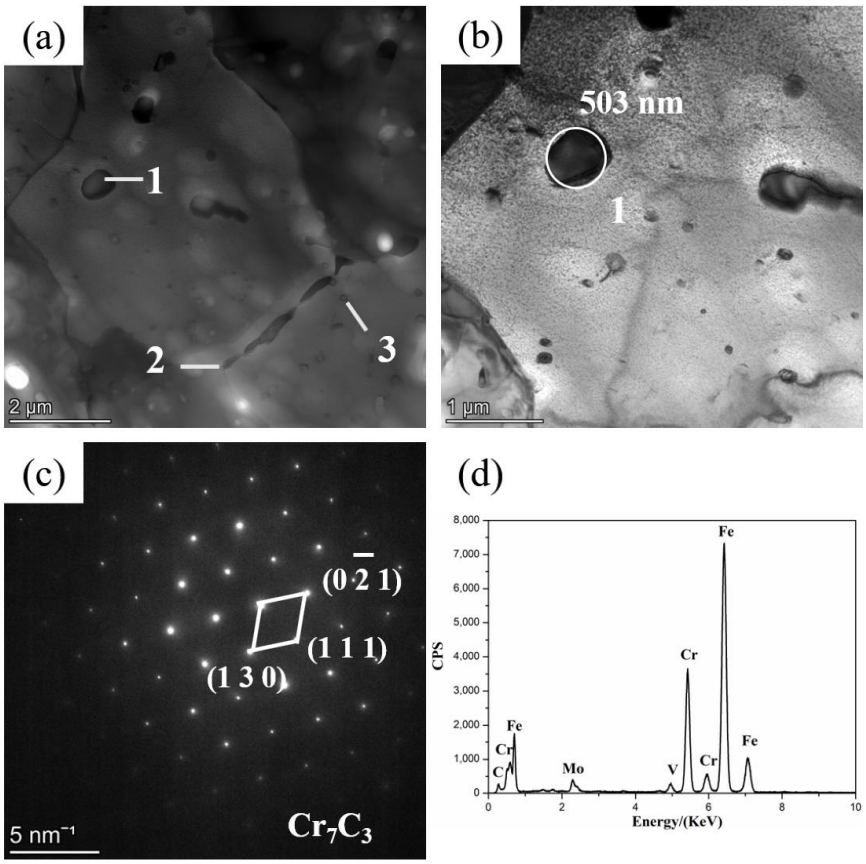


Figure 3. (**a**) TEM micrographs of carbides in RE-H13 die steel, (**b**) the morphology and (**c**) SAED patterns of intragranular carbides, (**d**) EDS analysis of Cr_7C_3 precipitates after annealing.

As shown in, to reveal the effects of RE on carbides distributed along the grain boundaries, the type and distribution of the carbides were investigated in detail. Figure 4a shows that a small number of carbides were distributed along the grain boundaries and most carbides were randomly distributed in the H13 die steel. As shown in Figure 4b, the effect of RE on the carbides along the grain boundaries was similar to Figure 2d, and the fraction of carbides perfectly aligned along the grain boundaries increased. This phenomenon also implies that the carbide precipitation can be affected by the microalloying of RE. In addition, combined with the SAED and EDS analysis, the type 2 carbide was identified as $Cr_{23}C_6$. As this carbide is precipitated mainly along the grain boundary, the reason for its chain distribution may be the segregation of RE and the decrease in interfacial energy at the grain boundary. However, the segregation of RE through EDS was not found at the grain boundary, which may be caused by a small amount added. Therefore, the effect of RE on the $Cr_{23}C_6$ carbide may be related to the nucleation at the grain boundary and the diffusion of carbon atoms in the process of precipitation.

Meanwhile, the type 3 nanoparticle carbides in RE-H13 die steel were observed using both TEM bright–field observation, high–resolution transmission electron microscopy, and fast Fourier transform in order to investigate the crystal structure and chemical composition, as shown in Figure 5. The distribution of the alloy element (V) was found through characterization analysis by mapping in Figure 5b. The result shows that the key alloy element is the V element in type 3 nanoparticle carbide and the size of the nanoparticle carbide was less than 200 nm. The results show that the particle in Figure 5b,c is the V(C,N) carbides with a cubic equiaxed crystal structure.

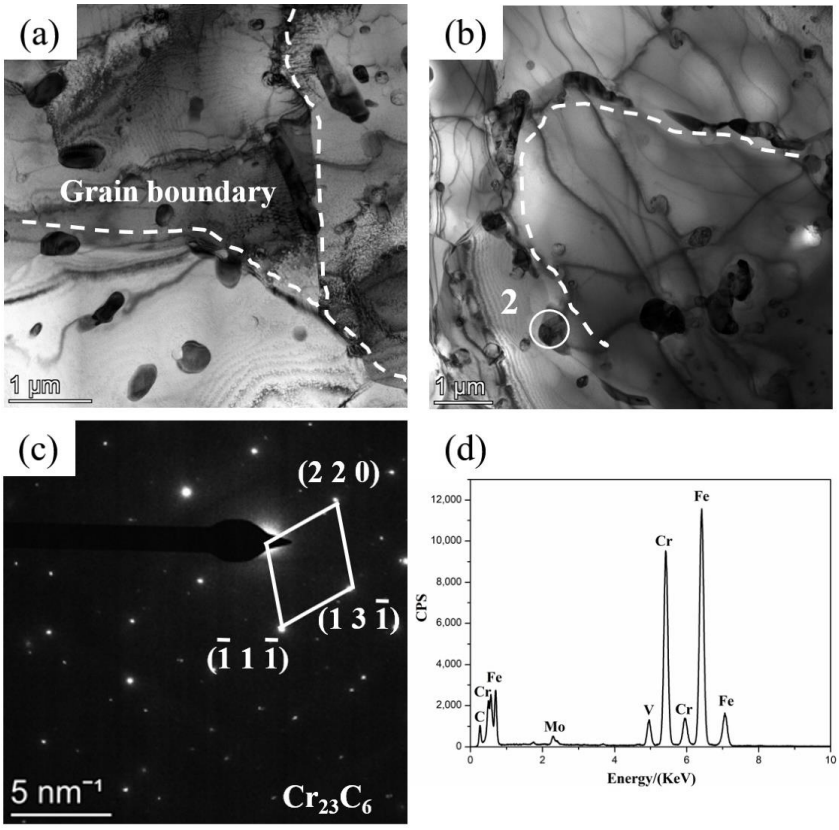


Figure 4. TEM micrographs of carbides in (**a**) H13 and (**b**) RE-H13 die steels, (**c**) SAED patterns of carbides along grain boundaries, (**d**) EDS analysis of $Cr_{23}C_6$ precipitates after annealing.

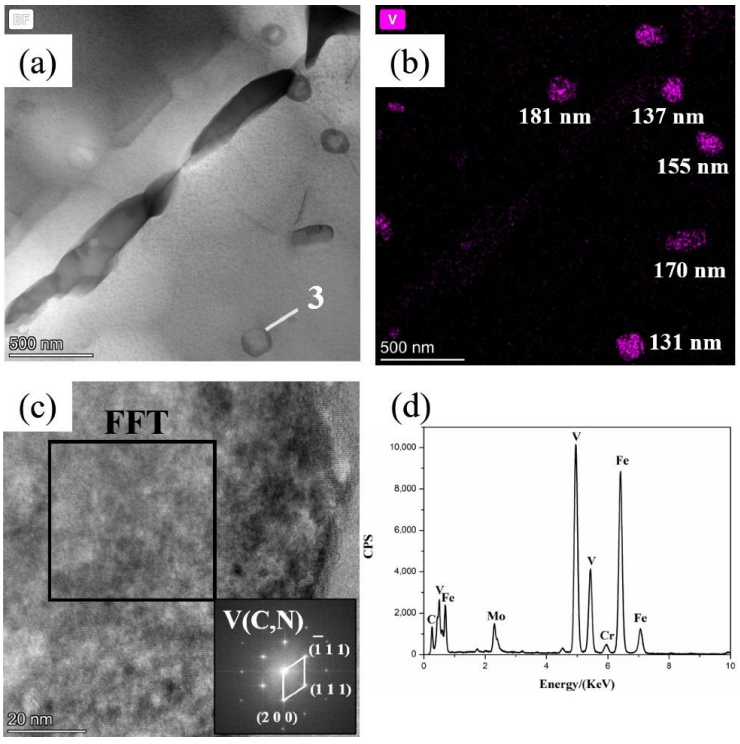


Figure 5. (**a**) Bright field micrographs of carbides in the RE-H13 die steel, (**b**) the distribution of V element, (**c**) HRTEM micrographs of the nano-scale carbide (the lower right inset shows the SAED patterns), (**d**) EDS analysis of V(C,N) precipitates after annealing.

3.3. *Effect of Rare Earth on Phase Transformation Point*

The difference between the transformation temperature was verified via thermal expansion tests. The thermal expansion curves of the two types of steel are shown in Figure 6, where the Ac_1 and Ac_3 temperatures of H13 die steel were 861.1 °C and 931.1 °C, respectively, and the Ac_1 and Ac_3 temperatures of RE-H13 die steel were 867.9 °C and 942.5 °C, respectively. The Ac_3 temperature of RE-H13 was 11.4 °C higher than that of the H13 die steel, and the Ac_1 temperatures were similar. The nature of the austenitization process revealed that the number of solid solution carbon atoms increased with increasing temperature. Therefore, the increase in the Ac_3 temperature of the RE-H13 die steel indirectly showed that the solid solution resistance of carbon atoms was increased and RE exerted a pinning effect on C atoms.

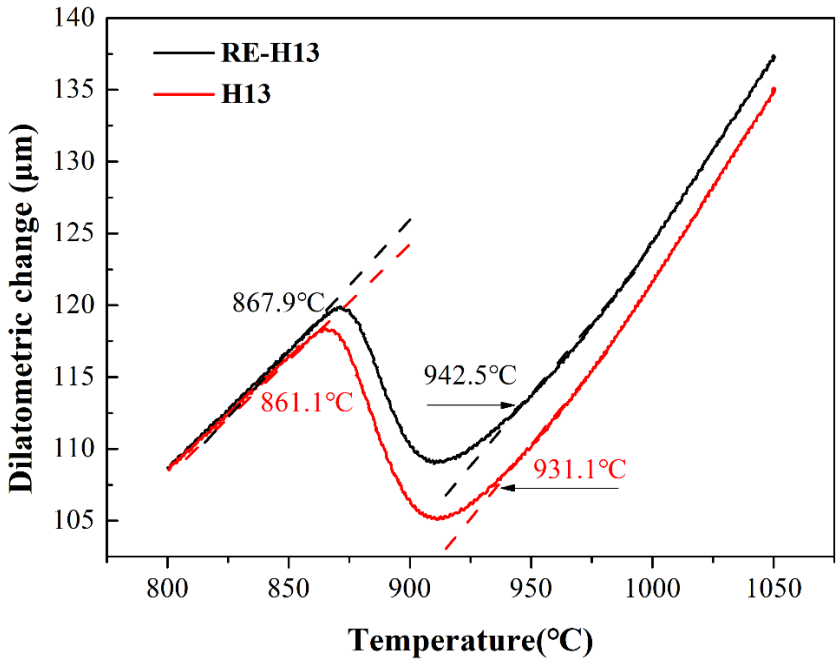


Figure 6. Thermal expansion curves of the tested steels after annealing.

The dimensions, morphology, and volumetric fraction of carbides play a critical role in improving the strength properties of the H13 die steel. This improvement results mainly from carbide precipitation (i.e., the primary carbides influence the uniformity of the microstructure and have a significant influence on the strength [20,21]). The cracks grow and spread (in general) around primary carbides [22]. The results of Figure 2d shows that the $Cr_{23}C_6$ carbides prefer to distribute along the grain boundaries in the RE-H13 die steel. The enhanced UTS resulting from the RE addition may be attributed to the differences among the primary carbides. The radius of the RE atoms is nearly 50% larger than that of the iron (Fe) atoms; hence, solid-solution formation is difficult, as evidenced by the segregation of the RE atoms at grain boundaries [11]. In both steel and magnesium alloys, these atoms typically form RE clusters at the grain boundaries, and the interface energy is reduced due to the segregation of RE at the grain boundaries [23]. Moreover, Jae observed (via a three-dimensional atom probe) the segregation of Cr, C, and RE at the same location along the grain boundaries [24]. Therefore, in the RE-H13 die steel, more Cr and C atoms were located near the grain boundaries than in other regions. As a result, the concentration of Cr and C atoms was decreased in the grain, and the precipitation of type 1 carbide was inhibited. As shown in Figure 2b (yellow arrow), a blank area appeared near the grain boundary. First-principles calculations revealed the affinity of RE to C [25]. In addition, RE segregation at the grain boundaries was observed in the RE-modified 51CrV4 spring steel, where the interaction between RE and carbon atoms was also characterized [26]. Combined with the phase transition results, these findings revealed that RE increased the resistance to phase transition, further confirming that RE

exerts a pinning effect on carbon diffusion. Furthermore, RE tends to segregate at the grain boundaries. Therefore, in the RE-H13 die steel, more carbon atoms were located near the grain boundaries than in other regions. Based on the segregation at the grain boundaries, a small fraction of solid solution RE was expected. Moreover, the lattice distortion near the grain boundaries was greater than in other regions due to the large difference between the radii of RE and Fe atoms. The reduction in the interface energy combined with the addition of RE may generate more nucleation sites for $M_{23}C_6$ carbides at the grain boundaries than in other regions. Hence, with the addition of RE, the fraction of $M_{23}C_6$ carbides increased along the grain boundaries. In addition, the segregation of RE purified the boundaries, thereby increasing the boundary strength. Moreover, RE can change the fracture mode (i.e., from intergranular fracture to transgranular fracture [27]). This resulted in hindering the migration of grain boundaries in the tensile process and improved grain boundary resistance to crack formation and propagation in the RE-H13 die steel and correspondingly, improved hardness and UTS of the steel. Nevertheless, the elongation decreased with an increased fraction of primary carbides along the grain boundary.

3.4. Effect of Rare Earth on Impact Fracture Morphology

Inclusions in steel typically induce "equator" cracks, break the continuity of matrix, and reduce the quality of the steels [28]. Compared to nonmetallic inclusions, the hardness of the spheroidal RE inclusions decreases and the melting point increases. Moreover, the thermal expansion coefficient and elastic modulus approach those of the steel matrix, thereby hindering the occurrence of stress concentrations [29]. The fracture morphology of the impact sample is shown in Figure 7. As shown in Figure 7a, the fracture of the H13 die steel showed brittle failure with a rugged river pattern. However, the fractography of the RE-H13 die steel showed quasi-cleavage fracture with dimples in Figure 7b, suggesting that the RE-H13 die steel exhibited both ductile and brittle fracture behavior. Moreover, the results in Figure 7c,d showed that there was a RE-inclusion near the dimples. This result indicates that RE promotes the transition of brittle-type failure to ductile-type failure. Notedly, there were some gaps between the inclusions and dimples, indicating that plastic deformation occurred during the fracture process. Meanwhile, RE-inclusion increased malleability in the process of necking. Therefore, the reduction in area remained unchanged with the decrease in the elongation rate.

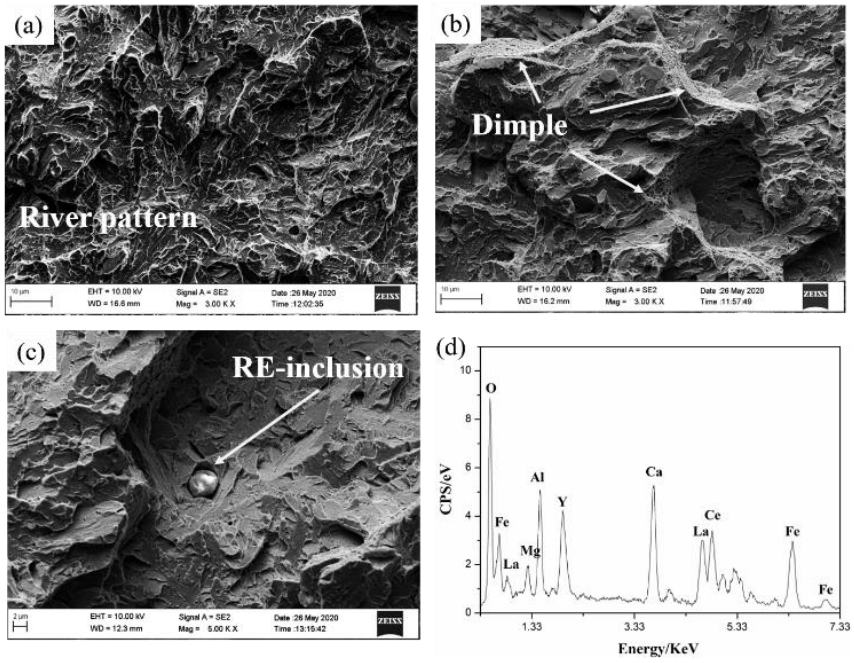


Figure 7. Impact fracture morphology of the tested steels: (**a**) H13 die steel; (**b**) and (**c**) RE-H13 die steel; (**d**) elemental analysis of RE-inclusion.

The impact toughness of H13 die steel depends mainly on the size and type of inclusions. Al_2O_3 and MnS inclusions can be easily broken during the application of a stress, resulting in small plastic deformation, and rapid crack propagation along the "equator". However, the RE inclusions are nearly spherical and deformation of these inclusions during the fracture process is difficult. The stress concentration generated during the crack propagation can therefore be alleviated and the propagation is impeded. Moreover, due to the modification of the inclusions, the reduction in area remains unchanged with increasing fraction of primary carbides along the grain boundary. Due to the high affinity of RE to oxygen and sulfur elements, the quality of the inclusions will change with the addition of RE. Moreover, Gao found that the misfit between Ce_2O_2S and the matrix was only 3.5%, and RE inclusions could become the core of heterogeneous nuclei [1]. Consequently, the modification of the RE-inclusions was reflected in the spheroidization of the inclusions and the small misfit with the matrix, which improves the impact toughness and provides the nucleation basis for precipitation strengthening in the RE-H13 die steel.

4. Conclusions

The effects of RE on the microstructure and mechanical properties of H13 steel were investigated. The major findings of this study can be summarized as follows:

1. With the addition of RE, the longitudinal impact energy and hardness increased by 43.7% and 6.9%, respectively, the UTS increased by ~50 MPa, the elongation rate decreased by 8%, and the reduction in area was almost constant.
2. The fraction of M23C6 carbides along the grain boundaries in the RE-H13 die steel was increased and hindered the migration of grain boundaries in the tensile process. The resistance to crack formation and propagation were improved in the RE-H13 die steel. In addition, due to the addition of RE, the Ac3 temperature increased by 11.4 °C, indicative of the RE-induced nailing effect on the carbon atoms.
3. RE can yield significant modification in the inclusions and improve inclusion resistance to crack formation and expansion. Therefore, RE promotes the transition of brittle–type failure to ductile–type failure and the reduction in area remains relatively constant.

Author Contributions: Conceptualization, Z.W. and R.C.; methodology, Z.W.; software, R.C.; validation, Z.W., J.H. and R.C.; formal analysis, F.Z.; investigation, R.C.; resources, Z.W; data curation, C.L.; writing—original draft preparation, R.C.; writing—review and editing, Z.W.; visualization, C.L.; supervision, Z.W.; project administration, Z.W.; funding acquisition, Z.W. All authors have read and agreed to the published version of the manuscript.

Funding: This research was funded by the Key Research and Development Program of Jiangxi Province (Grant No. 20192ACB50010, 20192BBEL50016) and the National Natural Science Foundation of China (Grant No. 51704132).

Acknowledgments: Longyi Heavy Rare Earths Co. Ltd. is also gratefully acknowledged for providing the raw materials and the RE alloy as well as Goal Science for its technical support in alloy smelting and processing.

Conflicts of Interest: The authors declare no conflicts of interest.

References

1. Gao, J.; Fu, P.; Liu, H.; Li, D. Effects of Rare Earth on the Microstructure and Impact Toughness of H13 Steel. *Metals* **2015**, *5*, 383–394. [CrossRef]
2. Rafi, H.K.; Ram, G.; Phanikumar, G.; Rao, K.P. Microstructural evolution during friction surfacing of tool steel H13. *Mater. Des.* **2011**, *32*, 82–87. [CrossRef]
3. Taktak, S. Some mechanical properties of borided AISI H13 and 304 steels. *Mater. Des.* **2007**, *28*, 1836–1843. [CrossRef]
4. Recco, A.A.C.; Tschiptschin, A.P. Structural and mechanical characterization of duplex multilayer coatings deposited onto H13 tool steel. *J. Mater. Res. Technol.* **2012**, *1*, 182–188. [CrossRef]
5. Das, K.; Alphonsa, J.; Ghosh, M.; Ghanshyam, J.; Rane, R.; Mukherjee, S. Influence of pretreatment on surface behavior of duplex plasma treated AISI H13 tool steel. *Surf. Interfaces* **2017**, *8*, 206–213. [CrossRef]

6. Hanghang, L.; Paixian, F.; Hongwei, L.; Chen, S.; Jinzhu, G.; Dianzhong, L. Carbides Evolution and Tensile Property of 4Cr5MoSiV1 Die Steel with Rare Earth Addition. *Metals* **2017**, *7*, 436.
7. Li, Y.; Liu, C.; Zhang, T.; Jiang, M.; Peng, C. Inclusions modification in heat resistant steel containing rare earth elements. *Ironmaking Steelmaking* **2016**, *45*, 76–82. [CrossRef]
8. Yang, C.; Luan, Y.; Li, D.; Li, Y. Effects of rare earth elements on inclusions and impact toughness of high-carbon chromium bearing steel. *J. Mater. Sci. Technol.* **2019**, *35*, 1298–1308. [CrossRef]
9. Yan, H.; Hu, Y.; Zhao, D. Influence of Rare Earth on Dynamic Recrystallization Behavior of As–Cast 30Mn Steel. *Adv. Mater. Sci. Eng.* **2018**, *2018*, 1–9. [CrossRef]
10. Zhang, X.; Wei, W.; Cheng, L.; Liu, J.; Wu, K.; Liu, M. Effects of niobium and rare earth elements on microstructure and initial marine corrosion behavior of low-alloy steels. *Appl. Surf. Sci.* **2019**, *475*, 83–93. [CrossRef]
11. Chen, L.; Ma, X.; Wang, L.; Ye, X. Effect of rare earth element yttrium addition on microstructures and properties of a 21Cr–11Ni austenitic heat–resistant stainless steel. *Mater. Des.* **2011**, *32*, 2206–2212. [CrossRef]
12. Pan, F.; Zhang, J.; Chen, H.L.; Su, Y.H.; Kuo, C.L.; Chen, S.H.; Lin, K.J.; Hsieh, P.H.; Hwang, W.S. Effects of Rare Earth Metals on Steel Microstructures. *Materials* **2016**, *9*, 417. [CrossRef] [PubMed]
13. Jiang, Z.; Wang, P.; Li, D.; Li, Y. Effects of rare earth on microstructure and impact toughness of low alloy Cr–Mo–V steels for hydrogenation reactor vessels. *J. Mater. Sci. Technol.* **2020**, *45*, 1–14. [CrossRef]
14. Zhou, X.; Yin, X.; Fang, F.; Jiang, J.; Zhu, W. Influence of rare earths on eutectic carbides in AISI M2 high speed steel. *J. Rare Earths* **2012**, *30*, 1075–1078. [CrossRef]
15. Fu, H.; Xiao, Q.; Li, Y. A study of the microstructures and properties of Fe–V–W–Mo alloy modified by rare earth. *Mater. Sci. Eng. A* **2005**, *395*, 281–287. [CrossRef]
16. Wang, S.Q.; Jiang, Q.C.; Cui, X.H.; He, Z.M. Influence of trace elements and heat treatment on carbide morphology and properties of CD-2 steel. *Mater. Sci. Eng. A* **1999**, *264*, 172–176. [CrossRef]
17. Hamidzadeh, M.A.; Meratian, M.; Saatchi, A. Effect of cerium and lanthanum on the microstructure and mechanical properties of AISI D2 tool steel. *Mater. Sci. Eng. A* **2013**, *571*, 193–198. [CrossRef]
18. Boccalini, M.; Correa, A.V.O.; Goldenstein, H. Rare earth metal induced modification of γ–M2C, γ–M6C, and γ–MC eutectics in as cast M2 high speed steel. *J. Mater. Sci. Technol.* **1999**, *15*, 621. [CrossRef]
19. Hufenbach, J.; Helth, A.; Lee, M.H.; Wendrock, H.; Giebeler, L.; Choe, C.Y.; Kim, K.H.; Kühn, U.; Kim, T.S.; Eckert, J. Effect of cerium addition on microstructure and mechanical properties of high–strength Fe85Cr4Mo8V2C1 cast steel. *Mater. Sci. Eng. A* **2016**, *674*, 366–374. [CrossRef]
20. Kang, M.; Park, G.; Jung, J. –G.; Kim, B.–H.; Lee, Y.–K. The effects of annealing temperature and cooling rate on carbide precipitation behavior in H13 hot–work tool steel. *J. Alloys Compd.* **2015**, *627*, 359–366. [CrossRef]
21. Hao, F.; Li, D.; Dan, T.; Ren, X.; Liao, B.; Yang, Q. Effect of rare earth oxides on the morphology of carbides in hardfacing metal of high chromium cast iron. *J. Rare Earths* **2011**, *29*, 168–172. [CrossRef]
22. Zhu, J.; Zhang, Z.; Xie, J. Improving strength and ductility of H13 die steel by pre–tempering treatment and its mechanism. *Mater. Sci. Eng. A* **2019**, *752*, 101–114. [CrossRef]
23. Sanaty–Zadeh, A.; Luo, A.A.; Stone, D.S. Comprehensive study of phase transformation in age–hardening of Mg–3Nd–0.2Zn by means of scanning transmission electron microscopy. *Acta Mater.* **2015**, *94*, 294–306. [CrossRef]
24. Seol, J.B.; Haley, D.; Hoelzer, D.T.; Kim, J.H. Influences of interstitial and extrusion temperature on grain 310 boundary segregation, Y−Ti−O nanofeatures, and mechanical properties of ferritic steels. *Acta Mater.* **2018**, *153*, 71–85. [CrossRef]
25. Gao, X.; Ren, H.; Wang, H.; Chen, S. Effect of lanthanum on the precipitation and dissolution of NbC in microalloyed steels. *Mater. Sci. Eng. A* **2017**, *683*, 116–122. [CrossRef]
26. Chen, R.; Wang, Z.; Zhu, F.; Zhao, H.; Qin, J.; Zhong, L. Effects of rare–earth micro–alloying on microstructures, carbides, and internal friction of 51CrV4 steels. *J. Alloys Compd.* **2020**, *824*, 153849. [CrossRef]
27. Zhu, J.; Xie, J.; Zhang, Z.; Huang, H. Microstructure and Obdurability Improvement Mechanisms of the La–Microalloyed H13 Steel. *Steel Res. Int.* **2018**, *89*, 1800044. [CrossRef]

28. Ahn, J. –H.; Jung, H.–D.; Im, J.–H.; Jung, K.H.; Moon, B.–M. Influence of the addition of gadolinium on the microstructure and mechanical properties of duplex stainless steel. *Mater. Sci. Eng. A* **2016**, *658*, 255–262. [CrossRef]
29. Jingpei, X.; Aiqin, W.; Wenyan, W.; Jiwen, L.; Luoli, L. Effects of Rare Earths on Toughness of 31Mn2SiRE Wear–Resistance Cast Steel. *J. Rare Earths* **2006**, *24*, 401–404. [CrossRef]



© 2020 by the authors. Licensee MDPI, Basel, Switzerland. This article is an open access article distributed under the terms and conditions of the Creative Commons Attribution (CC BY) license (http://creativecommons.org/licenses/by/4.0/).